Two-dimensional Cu(I)-MOF with mesoporous architecture towards chemiresistive NO_2 sensing

Dilip Pandey[a], Trivedi Samarth[a], Vikash Kumar Verma[b], Chandrabhan Patel[b], L Ponvijayakanthan[c], Neeraj K. Jaiswal[c*], Shaibal Mukherjee[b,d, e*] and Abhinav Raghuvanshi[a*]

[a]*Department of Chemistry, Indian Institute of Technology Indore, Madhya Pradesh 453552, India.*

[b]*Hybrid Nanodevice Research Group (HNRG), Department of Electrical Engineering, Indian Institute of Technology Indore, Madhya Pradesh 453552, India.*

[c]*2-D Materials Research Laboratory, Discipline of Physics, PDPM Indian Institute of Information Technology Design and Manufacturing, Jabalpur, Madhya Pradesh 482005, India*

[d]*Centre for Advanced Electronics (CAE), Indian Institute of Technology Indore, Madhya Pradesh 453552, India.*

[e]*School of Engineering, RMIT University, Melbourne, VIC 3001, Australia*

E-mail: ***neeraj@iiitdmj.ac.in, shaibal@iiti.ac.in, r.abhinav@iiti.ac.in***

Table of contents

General Information

1.1 Reagents

Materials required for the synthesis of DPA were purchased from Avra Chemicals. For ligand synthesis, TLC was used to monitor reaction progress using a Merck 60 F254 precoated silica gel plate (0.25 mm thickness), and the products were judged in a UV chamber. Both ^{1}H and $^{13}C\{^{1}H\}$ NMR spectra were collected using a Bruker 500 MHz spectrometer in DMSO-d^6. Data for proton NMR chemical shifts are shown in ppm downfield from tetramethyl silane and are mentioned in delta (δ) units. The ^{1}H NMR splitting patterns are singlet (s), doublet (d), triplet (t), and multiplet (m), and Mestre Nova processed the NMR data. Unless otherwise specified, chemicals were used exactly as received. CuI (>99%) from Loba Chemie Pvt. Ltd., and used without further purification. Solvents like diphenyl ether, acetonitrile (HPLC grade) were bought from Advent Chembio Pvt. Ltd.

Instruments

Powder X-ray diffraction (PXRD) data were recorded on Rigaku Smart X-ray diffractometer with monochromatic Cu Kα (0.1540 nm) radiation in 2θ range of 5-50 degrees. The attenuated total reflectance infrared spectroscopy (ATR-IR) was performed on Bruker Alpha II spectrophotometer of the powdered sample in the range of 4000-400 cm^{-1}. We have used a field

emission scanning electron microscope (FE-SEM) on JEOL JSM-7400F for morphological characterization and its elemental mapping. The thermogravimetric analysis was performed on Mettler Toledo TGA 1-star e-system in the temperature range of 30-700 °C.

Crystallographic details

Single crystal X-ray diffraction studies for **Cu-MOF** were carried out using Agilent technology (Oxford diffraction) super Nova CCD system, with monochromated Mo Kα radiation (λ=0.71073 Å). Unit cell determination, data collection and reduction, and empirical absorption correction were performed using the CrysAlisPro program. Using Olex2[1], the structure was solved with the SHELXT[2] structure solution program using Intrinsic phasing and refined with the SHELXL refinement package using Least Squares minimisation.

Sensing Measurements

5N purity gases such as (NO_2, NH_3, H_2S, SO_2, and CO_2) are employed to measure the sensing performance of the fabricated sensor. The flow rate of these gases is precisely controlled by using an advanced mass flow controller (model: Alicat, MC11 slpm, USA). The concentration of these test gases is varied by mixing the synthetic air (99.999 Purity) into the mixing chamber before exposing it on the sensor surface. The resistance change of the sensing layer during test gas exposure is continuously monitored on the Keithley-2612A source meter by applying a constant voltage of +1 V.

2.1 Synthesis of *N-phenyl-N-(pyridine-4-yl)pyridine-4-amine* (PDPA)

4,4'-Dipyridylamine (DPA) was synthesized following a previous report by Bureš *et al.*[3] For the synthesis of PDPA, in a two-neck r.b., DPA (2000 mg, 11.7 mmol) was added with $CuSO_4$(360 mg, 2.2 mmol), 18-crown-6 (120 mg, 0.05 mmol), potassium carbonate (3200mg, 23.4 mmol) with bromobenzene (3.6 mL, 34.8 mmol) in diphenyl ether (15 mL). The reaction temperature was maintained at 450K for two days in N_2. 2 days later, 200 mL of DCM and 200 mL of MeOH were added to the reaction mixture and passed through the celite pad. Most of the solvent was dried except diphenyl ether. Solvent and other impurities were removed and the compound was purified by column chromatography (Ph_2O and bromobenzene were removed by hexane as eluent and PDPA was obtained in ethyl acetate as eluent). (Yield:2000 mg, ~70%). **^{1}H NMR** (500 MHz, DMSO-d_6) δ 8.41 (s, 4H), 7.50 (t, *J* = 7.7 Hz, 2H), 7.37 (t, *J* = 7.6 Hz, 1H), 7.23 (d, *J* = 8.1 Hz, 2H), 6.95 (d, *J* = 4.7 Hz, 4H). **^{13}C{^{1}H} NMR** (126 MHz,

DMSO-d_6) δ 150.99, 150.16, 143.03, 129.92, 127.17, 126.52, 115.52. **LCMS** (ESI) *m/z* calculated for **C**$_{16}$H$_{13}$N$_3$ [M+H]$^+$ 248.1182, found 248.1201.

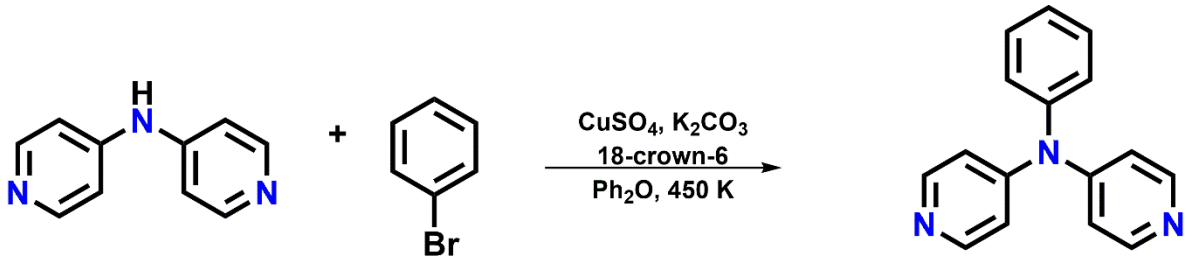

Scheme S1. Synthesis of PDPA

2.2 ATR-IR of PDPA

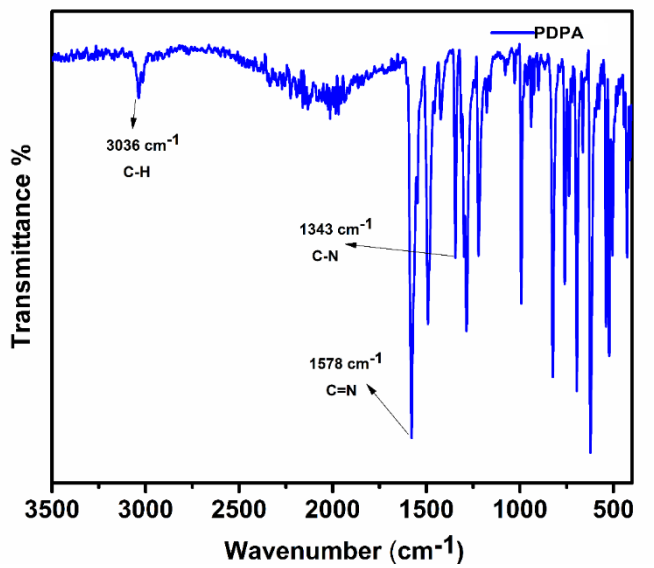

Figure S1. IR spectra of PDPA

2.3 Mass spectra of PDPA

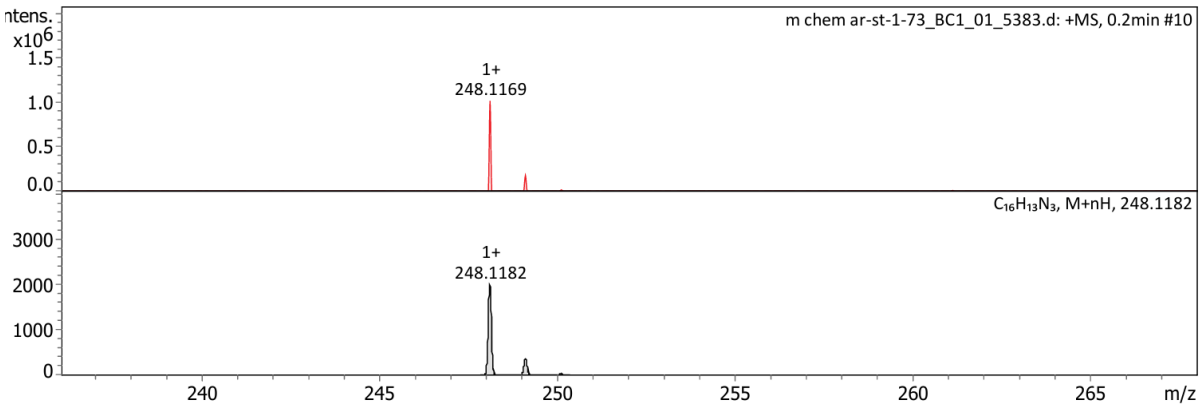

Figure S2. Mass spectra of PDPA

2.4 NMR spectra of PDPA

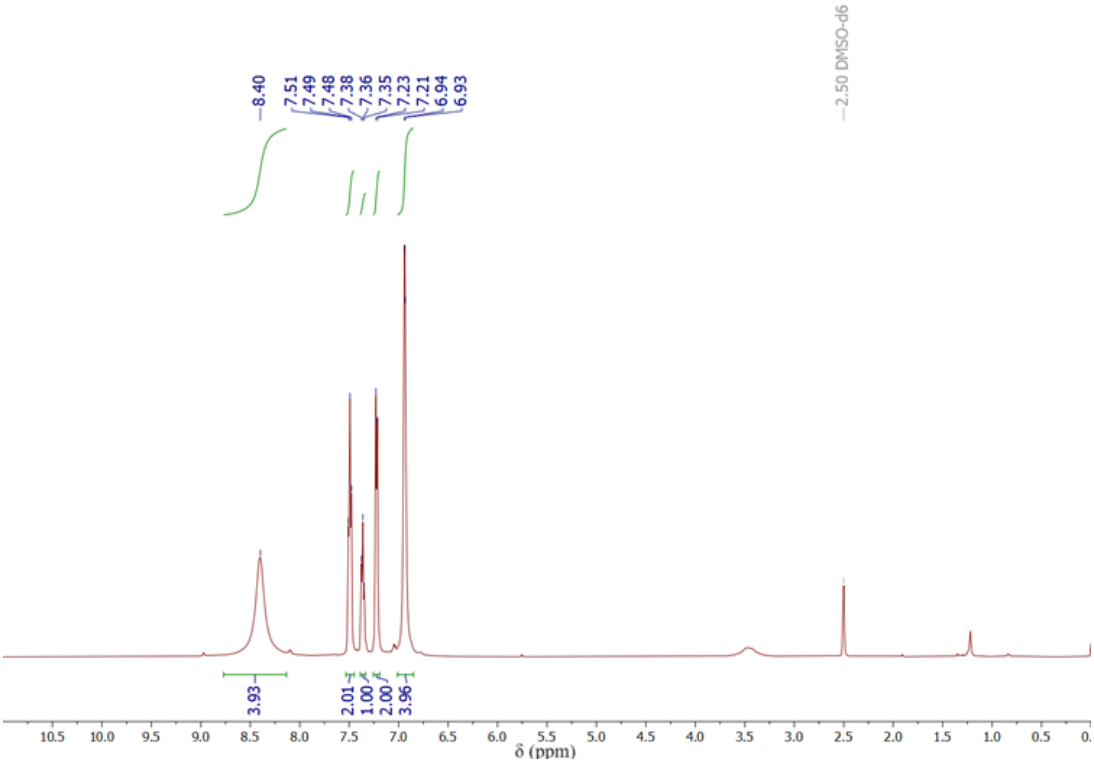

Figure S3. ^{1}H NMR of PDPA

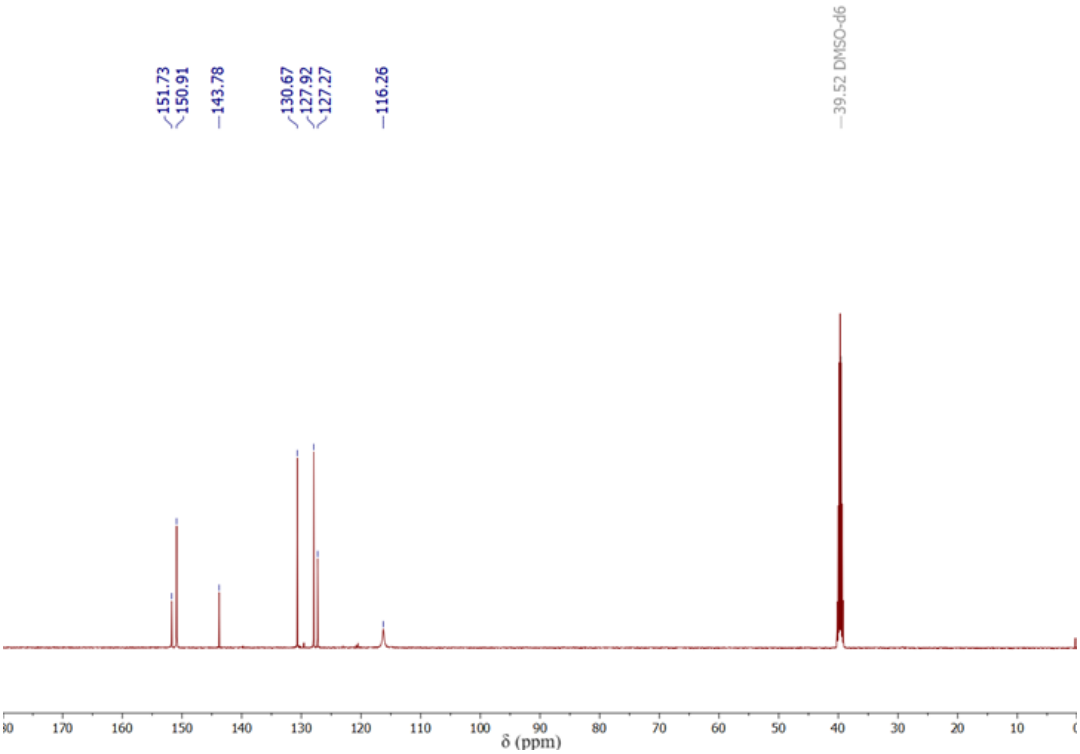

Figure S4. ^{13}C{^{1}H} NMR of PDPA

2.5 Synthesis of **Cu-MOF**

Into a 50 mL Schenk tube under N_2 condition, PDPA (100 mg, 0.8 mmol) was dissolved in 2mL DCM, to which CuI (153 mg, 1.6 mmol) dissolved in 10 mL ACN was added and resulted in instant white precipitates. The reaction mixture was stirred for 12 hours, after which the compound was dried and washed with ACN. (Yield: 200 mg, ~80%). Crystals were obtained by slow diffusion of CuI dissolved in ACN over ligand dissolved in DCM.

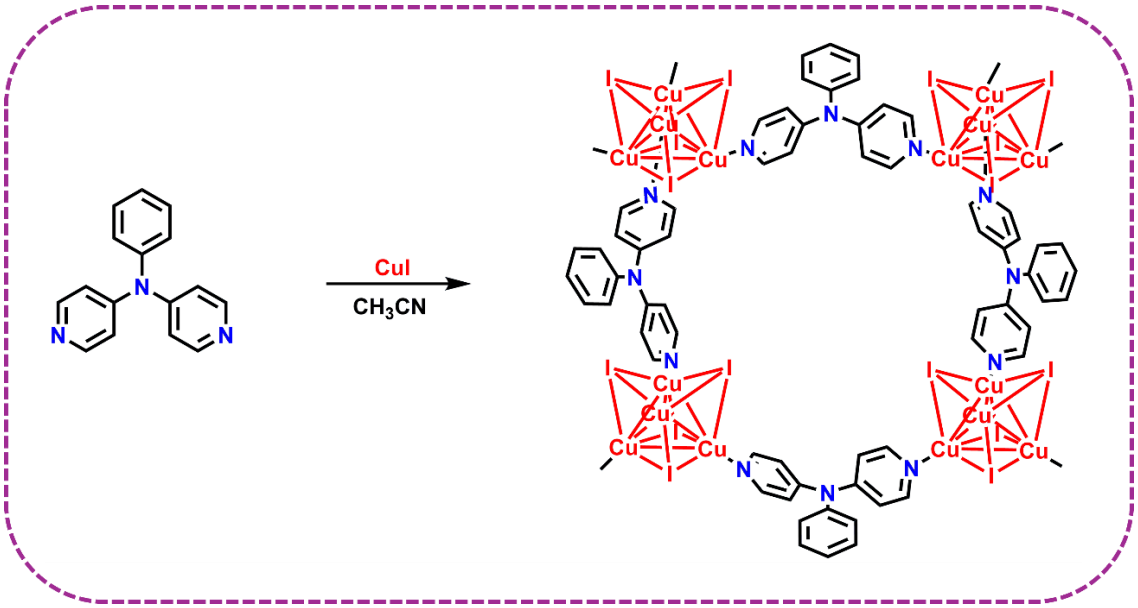

Scheme S2. Synthesis of **Cu-MOF**

2.6 ATR-IR of **Cu-MOF**

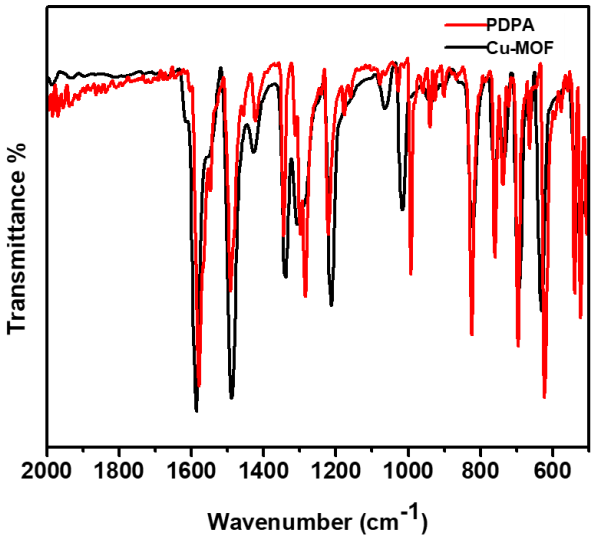

Figure S5. Comparison of IR spectra of PDPA and **Cu-MOF**

3.1 Structure of **Cu-MOF**

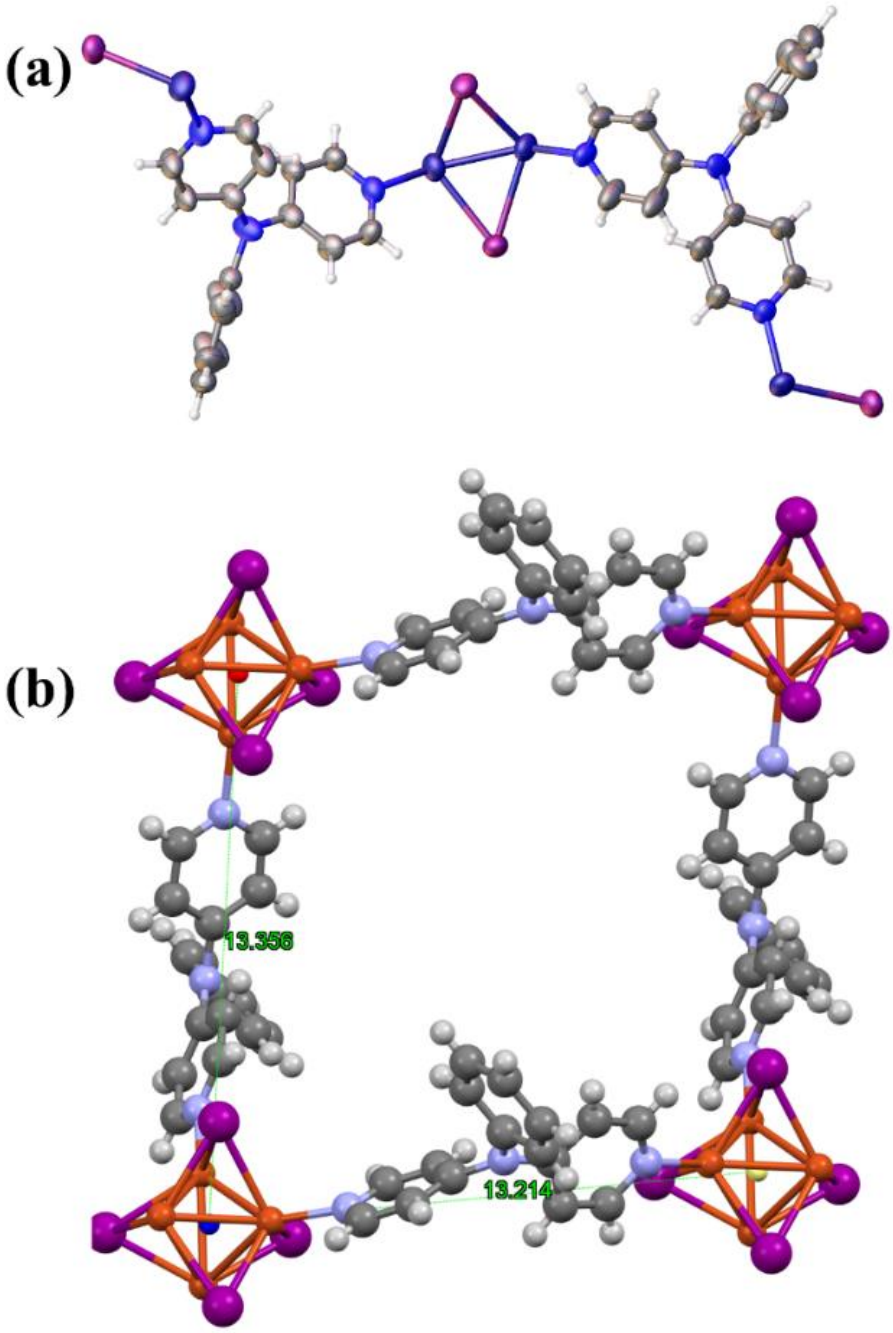

Figure S6. (a) The asymmetric unit of **Cu-MOF** (b) different lengths across axes

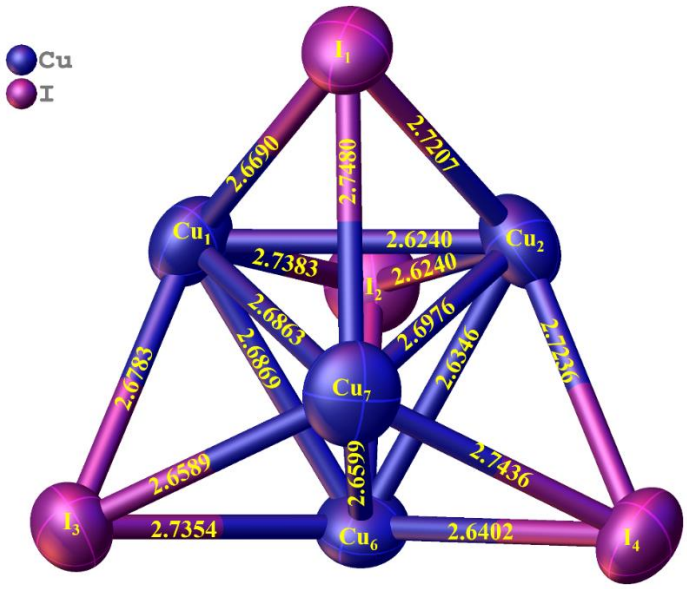

Figure S7. Bond lengths of Cu-Cu and Cu-N in Cu_4I_4 SBU

3.2 PXRD and TGA of **Cu-MOF**

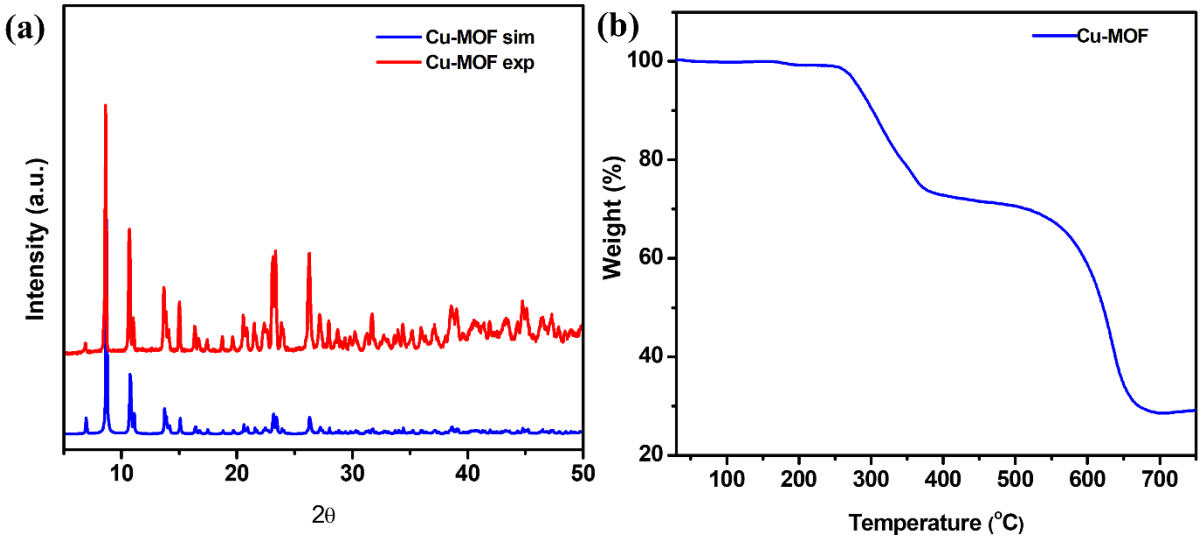

Figure S8. (a) PXRD patterns of Simulated and experimental **Cu-MOF** (b) TGA curve of **Cu-MOF**

3.3 Crystallographic parameters of **Cu-MOF**

Table S1. Crystallographic table

Compound	**Cu-MOF**
CCDC No.	2385865
Formula	$C_{35}H_{31}Cl_2Cu_4I_4N_7$
Formula Weight	1382.33
Wavelength	0.71073 Å
Crystal System	monoclinic
Space group	*Cc*
a/Å	16.9593(2)
b/ Å	20.2694(2)
c/ Å	13.3565(2)
α /°	90
β/°	105.5110(10)
γ/°	90
V/ Å^3	4424.14(10)
Z	4
ρ_{calcd} (g/cm^3)	2.075
Temperature/K	298.00
GOF	1.034
2θ range for data collection	4.006 to 54.814
Reflections collected	70029
Independent reflections	9468 [R_{int} = 0.0377, R_{sigma} = 0.0283]
Completeness to θ=25.242	99.8
Final R indices [I>2σ(I)]	R_1 = 0.0345, wR_2 = 0.0766
Final R indices [all data]	R_1 = 0.0416, wR_2 = 0.0801
Largest diff. peak/hole/ e Å^{-3}	0.48/-0.52

3.4 Surface analysis of **Cu-MOF**

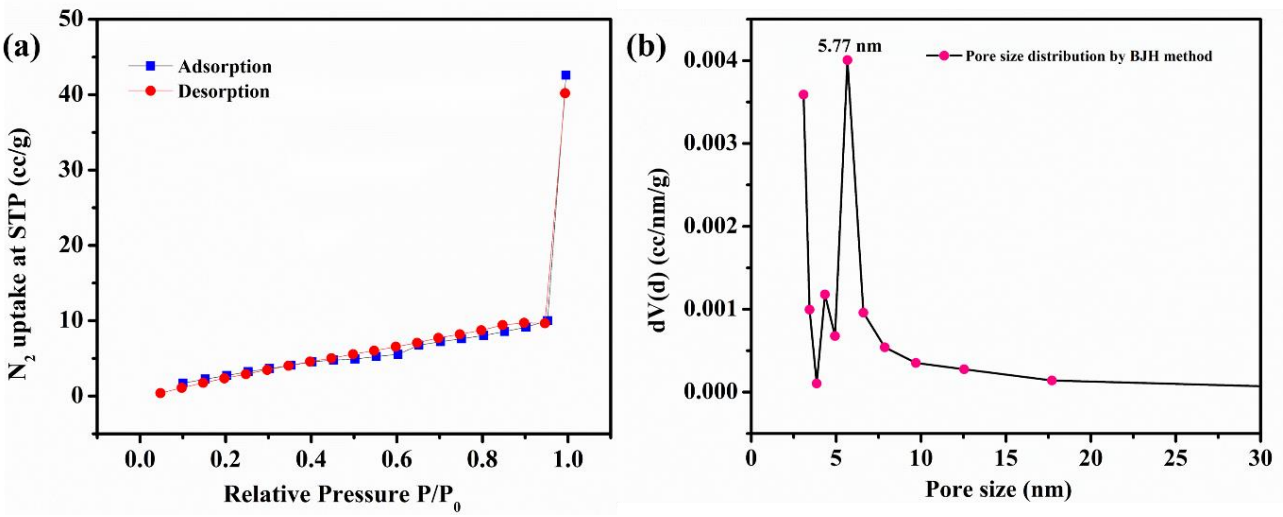

Figure S9. (a) BET (b) BJH of **Cu-MOF**

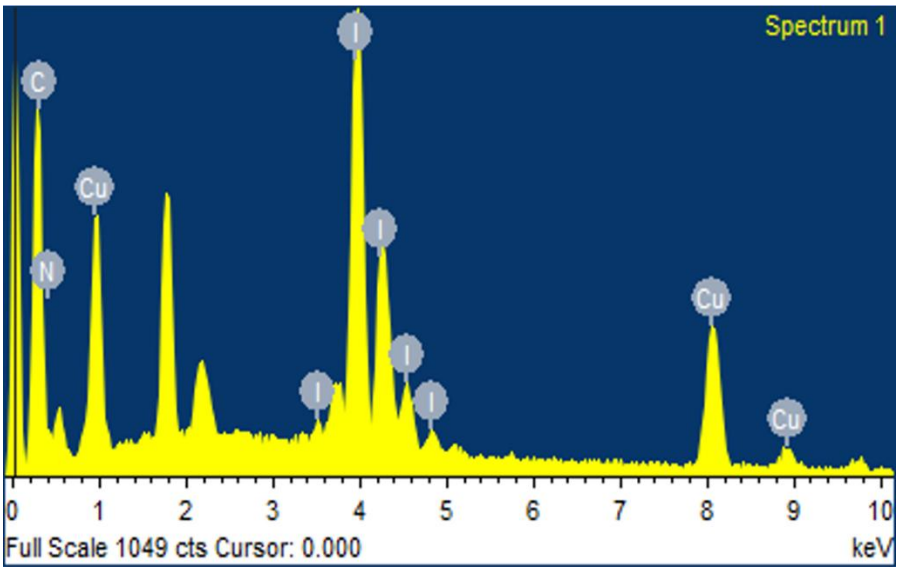

Figure S10. Energy Dispersive X-ray of **Cu-MOF**

3.5 Semiconducting Behaviour of **Cu-MOF**

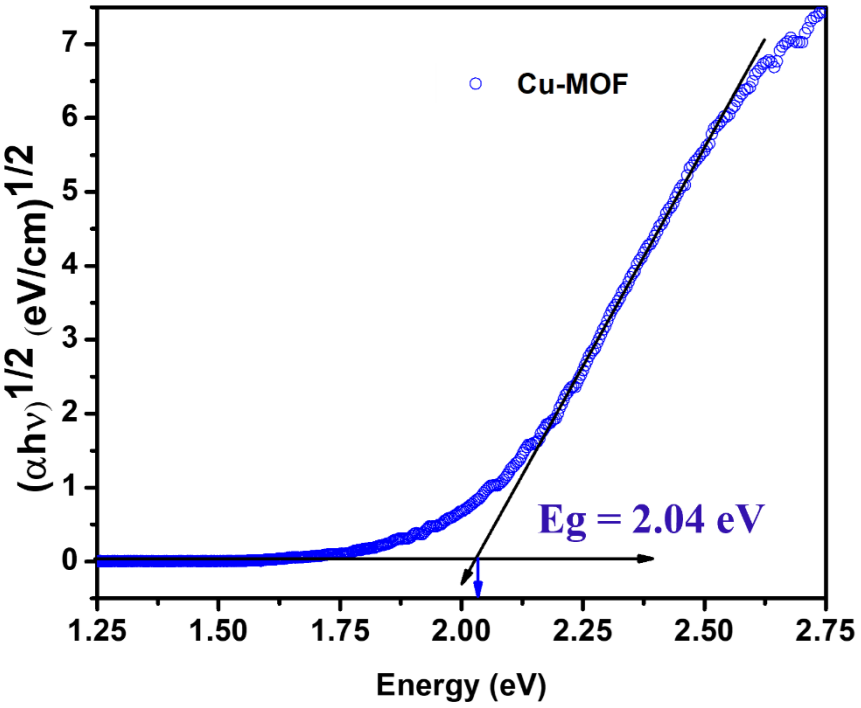

Figure S11. Tauc-Plot of **Cu-MOF**

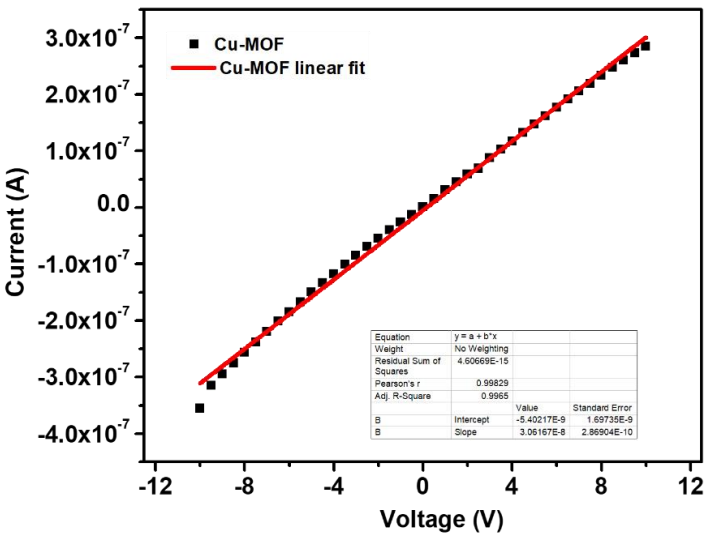

Figure S12. Electrical Conductivity of **Cu-MOF**

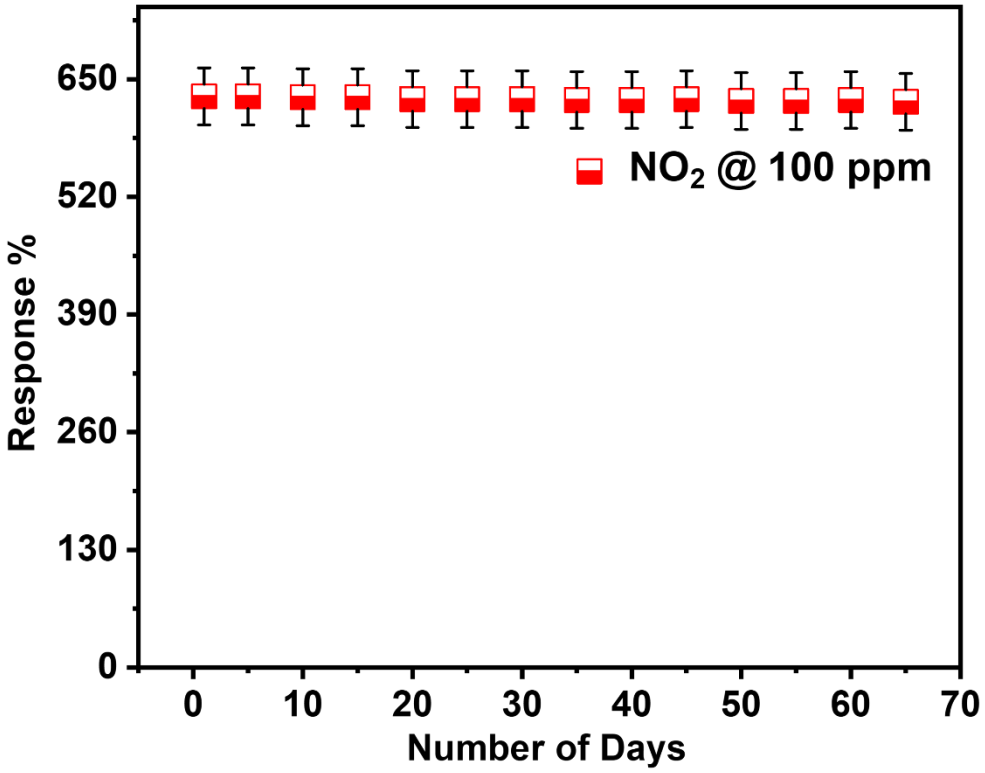

Figure S13. Long-term stability of **Cu-MOF**-based gas sensor

4.1 Gas sensing behavior of **Cu-MOF**

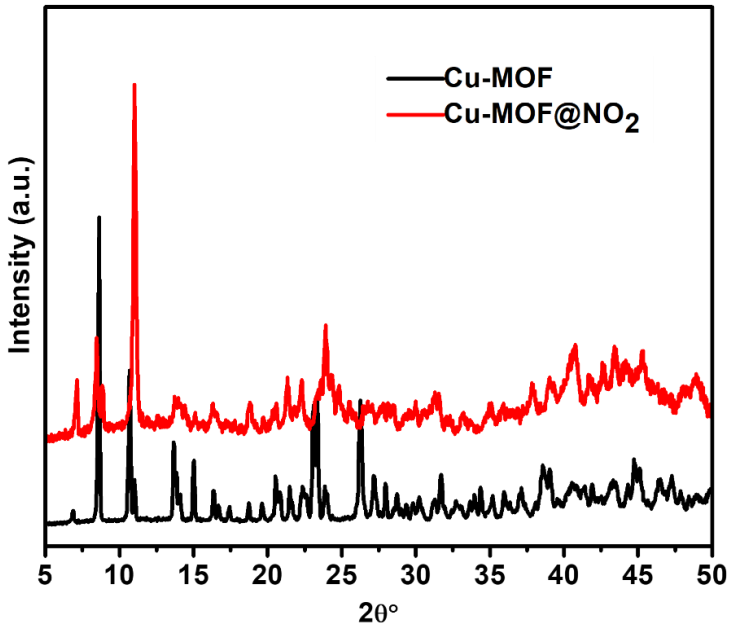

Figure S14. Comparison of PXRD patterns of **Cu-MOF** before and after exposure to NO_2

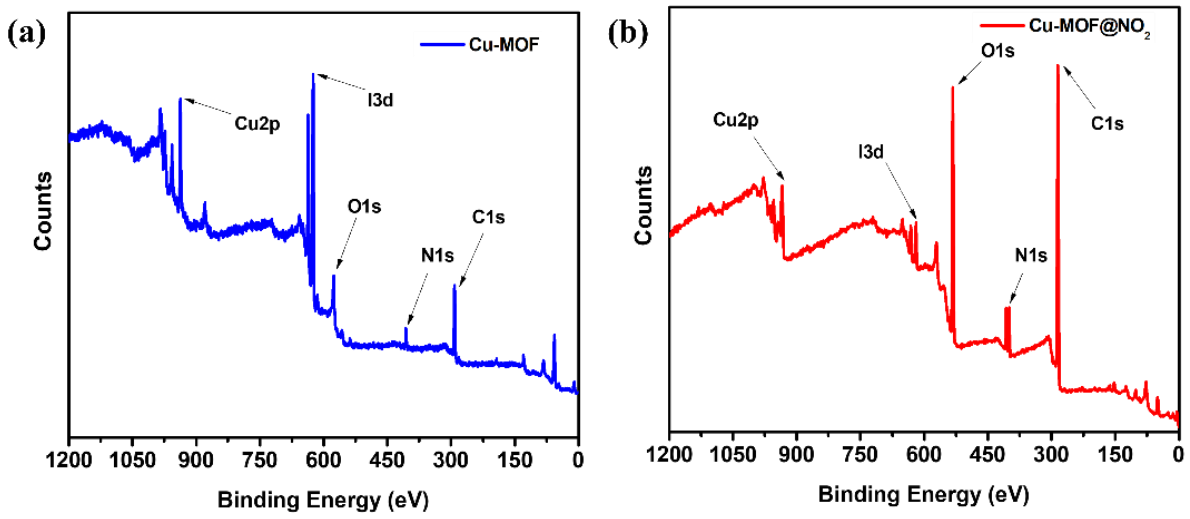

Figure S15. (a) XPS survey of **Cu-MOF** (b) XPS survey of **Cu-MOF** after NO_2 exposure.

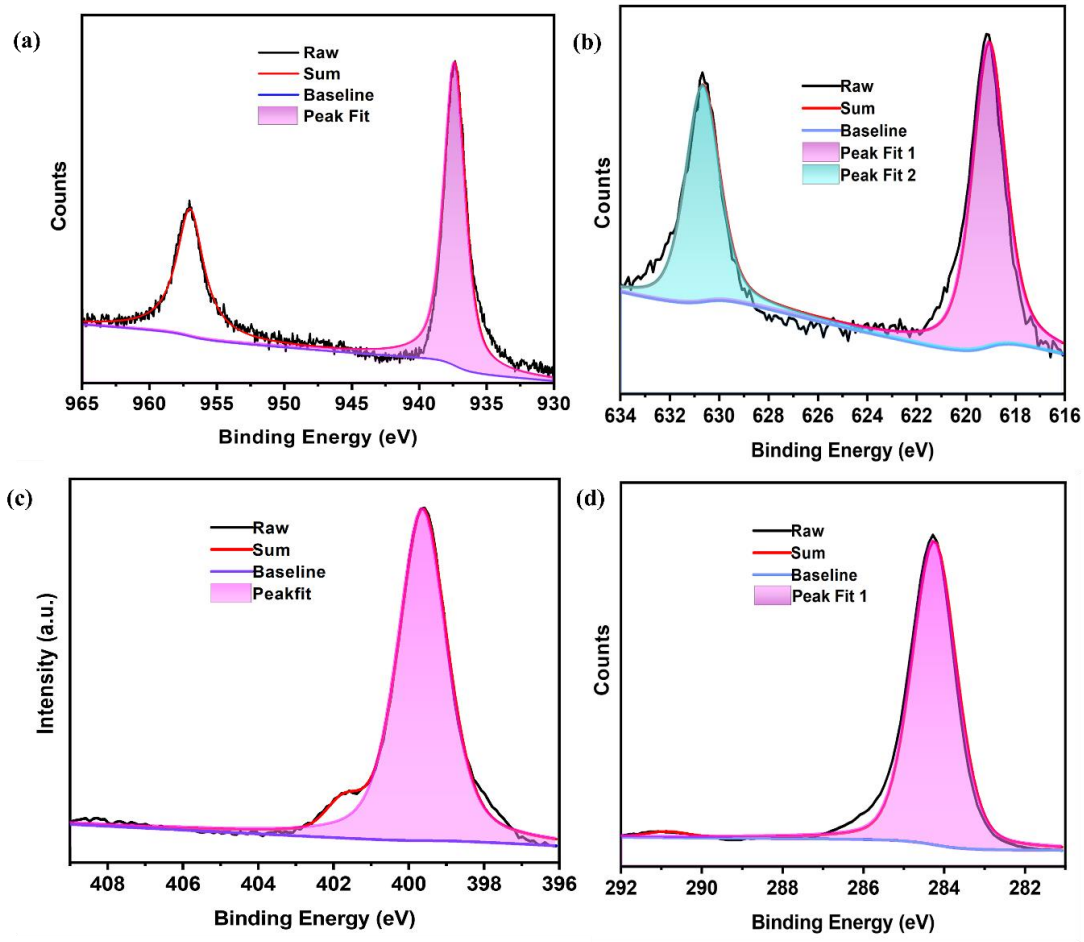

Figure S16. High-resolution XPS spectra of **Cu-MOF** (a) Cu2p (b) I3d (c) N1s (d) C1s

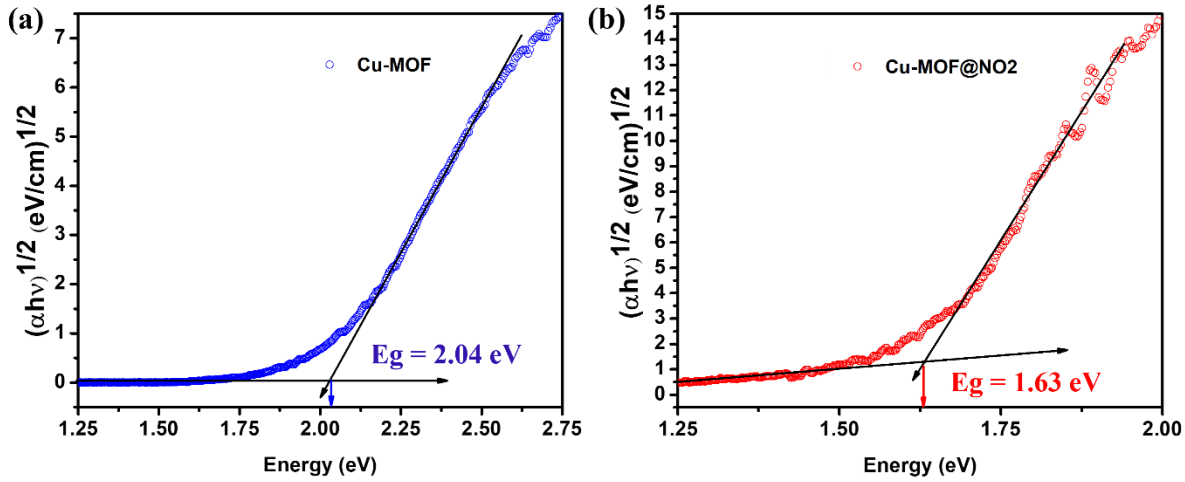

Figure S17. Tauc-Plot of **Cu-MOF** (a) before exposure to NO_2 (b) after exposure to NO_2

4.2 Comparison of **Cu-MOF** as a gas sensor

Table S2. Comparison table for NO_2 gas sensing with MOF-based sensor at room temperature.

Serial No.	Sensing material	Conc. (ppm)	Response /Recovery time (s)	LOD #	References
1.	Cu-Salphen-MOF	10	135/412.2	0.28 ppm	*Angew. Chem. Int. Ed.*, 2023, **62**, e202302645
2.	$Cu_3(HHTP)_2$	1	1080/--	--	*Adv. Sci.*, 2019, **6**, 1900250
3.	HIOTP-Ni	10	101.4/619.2	0.21 ppm	*Angew. Chem.*, 2023, **135**, e202306224
4.	$Zn_3(HHTQ)_2$	3	132/594	0.269 ppm	*Angew. Chem. Int. Ed.*, 2024, **35**, e202408189
5.	CuI-K-INA	10	121.8/312.6	14.12 ppb	*J. Am. Chem. Soc.*, 2023, **145**, 19293–19302
6.	$Cu_3(HHTP)_2$ powder	3	1038/--	1 ppm	*Nat. Commun.*, 2021, **12**, 4294
7.	PCN-222-Cu	0.02	67/261	0.93 ppb	*ACS Sens.*, 2023, **8**, 4353–4363
8.	PCN-222-Ni	0.15	82/159	5.98 ppb	*ACS Sens.*, 2023, **8**, 4353–4363
9.	Cu(I) CP	10	15.5/21	1.3 ppb	*Small*, 2025, 2409553
10.	**Cu-MOF**	**10**	**11.6/13**	**3.5 ppb**	**This Work**

Table S3. Comparison table for NO_2 gas sensing with hybrid MOF-based sensor at room temperature.

Serial No.	Sensing material	Conc. (ppm)	Response /Recovery time (s)	LOD[#]	References
1.	$Ni_3(HHTP)_2$/ polyimide (PI), tape (PET)	0.2	--/30	56 ppb	*ACS Sens.*, 2024, **9**, 1916–1926
2.	Au/ZIF-8-film	10	7.2/ > 600	0.19 ppm	*ACS Appl. Mater. Interfaces*, 2019, **11**, 13624–13631
3.	$Cu_3(HHTP)_2$-NFs	5	~ 600/~ 600	--	*ACS Cent. Sci.*, 2021, **7**, 1176–1182
4.	$Cu_3(HHTP)_2/Fe_2O_3$	5	~ 600/~ 600	11 ppb	*ACS Cent. Sci.*, 2021, **7**, 1176–1182
5.	$Cu_3(HHTP)_2$ Thin film	3	840/--	1 ppm	*Nat. Commun.*, 2021, **12**, 4294
6.	MIL-101(Cr)⊃ PEDOT	10	150/Irr.	0.06 ppm	J. Am. Chem. Soc. *138*, 10088–10091
7.	LIG@$Cu_3(HHTP_2)$	0.01	16/15	0.168 ppb	*Nat. Commun.*, 2023, **14**, 3114
8.	Pd@$Cu_3(HHTP)_2$	5	828/--	1ppm	*Adv. Sci.*, 2019, **6**, 1900250
9.	Thin film Pt@$Cu_3(HHTP)_2$	3	492/--	0.1 ppm	*Nat. Commun.*, 2021, **12**, 4294
10.	**Cu-MOF**	**10**	**11.6/13**	**3.5 ppb**	**This Work**

#:- LOD values are determined by (3*SD/σ) where, SD represents the deviation of sensor response values obtained in the presence of air, while σ represents the slope of the linear portion of the calibrated curve.

4.3 Theoretical calculations of **Cu-MOF**

Table S4. The calculated Mulliken charges (in e) before and after adsorption on NO_2 molecule and Cu-I complex of **Cu-MOF**

	Atom	Before adsorption	After Adsorption
Cu-MOF	Cu1	18.744	18.582
	Cu2	18.750	18.682
	Cu3	18.739	18.694
	Cu4	18.750	18.758
	I1	7.317	7.280
	I2	7.338	7.332
	I3	7.336	7.291
	I4	7.310	7.283
Adsorbate NO_2 molecule	N	4.897	5.002
	O	6.050	6.231
	O	6.053	6.225

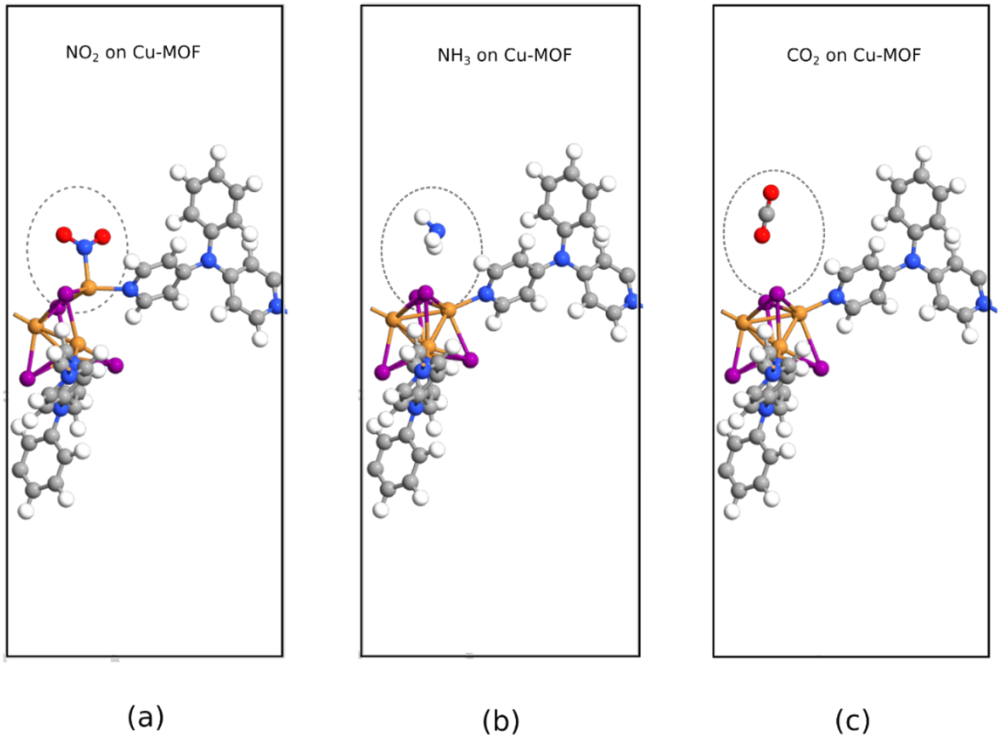

Figure S18. Interaction of **Cu-MOF** with (a) NO_2 (b) NH_3 (c) CO_2

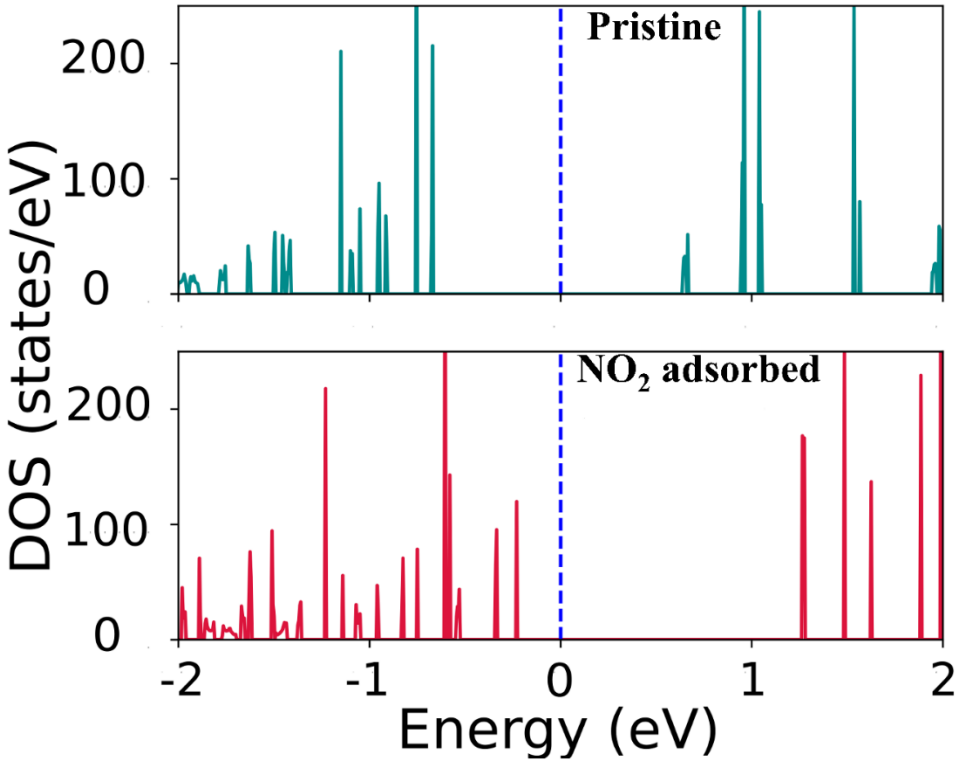

Figure S19. DOS of prinstine and adsorbed NO_2 on **Cu-MOF**

References:

1 O. V. Dolomanov, L. J. Bourhis, R. J. Gildea, J. A. K. Howard and H. Puschmann, *J Appl Crystallogr*, 2009, **42**, 339–341.
2 G. M. Sheldrick and T. R. Schneider, in *Methods in Enzymology*, Elsevier, 1997, vol. 277, pp. 319–343.
3 F. Bureš, D. Cvejn, K. Melánová, L. Beneš, J. Svoboda, V. Zima, O. Pytela, T. Mikysek, Z. Růžičková, I. V. Kityk, A. Wojciechowski and N. AlZayed, *J. Mater. Chem. C*, 2016, **4**, 468–478.
4 X. Su, Z. Zhong, X. Yan, T. Zhang, C. Wang, Y.-X. Wang, G. Xu and L. Chen, *Angewandte Chemie International Edition*, 2023, **62**, e202302645.
5 Y.-M. Jo, K. Lim, J. W. Yoon, Y. K. Jo, Y. K. Moon, H. W. Jang and J.-H. Lee, *ACS Cent. Sci.*, 2021, **7**, 1176–1182.
6 B. Le Ouay, M. Boudot, T. Kitao, T. Yanagida, S. Kitagawa and T. Uemura, *J. Am. Chem. Soc.*, 2016, **138**, 10088–10091.